RESEARCH ARTICLE

CHROMATIN SEQUENCING

Single-molecule regulatory architectures captured by chromatin fiber sequencing

Andrew B. Stergachis[1]*, Brian M. Debo[1,2], Eric Haugen[3], L. Stirling Churchman[2], John A. Stamatoyannopoulos[3,4]*

Gene regulation is chiefly determined at the level of individual linear chromatin molecules, yet our current understanding of cis-regulatory architectures derives from fragmented sampling of large numbers of disparate molecules. We developed an approach for precisely stenciling the structure of individual chromatin fibers onto their composite DNA templates using nonspecific DNA N^6-adenine methyltransferases. Single-molecule long-read sequencing of chromatin stencils enabled nucleotide-resolution readout of the primary architecture of multikilobase chromatin fibers (Fiber-seq). Fiber-seq exposed widespread plasticity in the linear organization of individual chromatin fibers and illuminated principles guiding regulatory DNA actuation, the coordinated actuation of neighboring regulatory elements, single-molecule nucleosome positioning, and single-molecule transcription factor occupancy. Our approach and results open new vistas on the primary architecture of gene regulation.

The primary architecture of chromatin comprises nucleosome arrays punctuated by short regulatory regions containing transcription factors (TFs) and other non-histone proteins. This architecture is foundational for genome function yet remains undefined at the level of individual chromatin fibers, the fundamental units of gene regulation. For example, it is largely unknown how regulatory DNA is actuated on individual chromatin fibers, or the degree to which nearby regulatory regions are coordinately actuated on the same chromatin fiber. It is also unknown how regulatory DNA actuation affects nucleosome positioning on individual chromatin fibers, and how TF occupancy modulates regulatory DNA actuation and function on single templates. Addressing these questions requires nucleotide-resolution analysis of individual multikilobase chromatin fibers, which is not obtainable with current single-cell or bulk profiling approaches.

We sought to develop a method for recording the primary architecture of chromatin onto its underlying DNA template at single-nucleotide resolution, thereby enabling the simultaneous identification of genetic and epigenetic features along multikilobase segments of the genome. Current approaches to mapping chromatin and regulatory architectures sample large populations of chromatin fibers and rely on dissolution of chromatin using nucleases such as deoxyribonuclease (DNase I) (*1*, *2*), micrococcal nuclease (*3*, *4*), restriction enzymes (*5*), transposases (*6*), or mechanical shearing (*7*). CpG and GpC methyltransferases are capable of marking accessible cytosines in a dinucleotide context without digesting DNA (*8*–*10*), and approaches using GpC methyltransferases have been extended to single-pass nanopore sequencing (*11*, *12*). However, the utility of these approaches for gaining insights into the biology of individual chromatin fibers is limited because of (i) the sporadic occurrence and linear clustering of CpG and GpC dinucleotides in animal genomes as a result of mutation and selection (fig. S1); (ii) the confounding influence of endogenous cytosine methylation machineries (*13*); (iii) the marked DNA degradation induced by bisulfite conversion (*14*); and (iv) the intrinsically limited ability of nanopore sequencing to accurately identify modified bases on a per-molecule basis (*11*, *12*, *15*).

Unlike cytosine, adenine bases in DNA are almost completely devoid of endogenous methylation in eukaryotes (*16*) and occur at an average frequency approaching one in every two DNA base pairs in animal genomes without the clustering and extended deserts characteristic of guanine-cytosine dinucleotides (fig. S1). The sequence-specific adenine methyltransferase *Dam* demonstrates some preference for nonchromatinized DNA (*17*–*19*), suggesting that nonspecific members of this class of enzymes could have similar properties. We therefore sought to identify a nonspecific (that is, non–sequence context dependent) N^6-adenine DNA methyltransferase (m6A-MTase) with high efficiency, high stability, and a molecular weight similar to that of nonspecific nucleases such as DNase I (~30 kD) that are able to access protein-DNA interfaces at nucleotide resolution (Fig. 1A). We isolated five distinct nonspecific DNA m6A-MTases (*20*–*23*) and demonstrated that treatment of nonchromatinized (fig. S2) and chromatinized DNA templates (Fig. 1B) with increasing amounts of each enzyme resulted in monotonic increases in adenine methylation.

m6A-MTases are quantitative probes of DNA accessibility

To establish selectivity of nonspecific m6A-MTases for accessible DNA templates in nuclear chromatin, we treated *Drosophila melanogaster* S2 cell nuclei with increasing concentrations of five adenine methyltransferases and compared the genomic distribution of m6A-DNA with the distribution of DNase I cleavages, defined using DNase I–seq [the established standard for marking accessible DNA templates (*1*, *2*)] (Fig. 1C). Immunoprecipitation and sequencing of short [median, 110 base pairs (bp)] DNA fragments harboring m6A (AdMTase-seq) showed the genomic distribution of m6A-DNA to mirror the density of DNase I cleavages quantified by DNase I–seq (Fig. 1D). m6A-MTases showed high selectivity for accessible DNA and quantitative representation of DNase I–hypersensitive sites (DHSs) (Fig. 1D and fig. S3). Further, m6A-MTases demonstrated decreasing selectivity toward DHSs with increasing amounts of enzyme (Fig. 1E and fig. S3, A and B), analogous with the enzymatic action of DNase I (or micrococcal nuclease) on chromatin substrates due to increasing marking of the far more numerous internucleosomal linker regions (*24*–*26*). Quantification of DNA accessibility by AdMTase-seq was highly reproducible at both promoter-proximal and promoter-distal regulatory elements (Fig. 1F and fig. S3C), with the enzyme Hia5 demonstrating the highest efficiency (figs. S2 and S3). These results show that nonspecific m6A-MTases provide quantitative probes of DNA accessibility in chromatin.

m6A stencils reveal single-molecule chromatin architectures

We next aimed to reconstruct the primary architecture of chromatin fibers at nucleotide resolution by sequencing the linear pattern of m6a along multikilobase chromatin stencils; we termed this process Fiber-seq (Fig. 2A). To implement Fiber-seq, we capitalized on the ability of single-molecule DNA sequencers to discriminate methylated from unmethylated adenine residues based on the DNA polymerase kinetics at that base during sequencing (*23*, *27*). To achieve nucleotide resolution, we leveraged single-molecule circular consensus sequencing (CCS) (*27*, *28*) performed on a Pacific Biosciences (PacBio) instrument, which enables resequencing of each chromatin fiber stencil at least 10 times, resulting in highly accurate base calling of both modified and unmodified nucleotides.

To create chromatin stencils, we performed m6A-MTase treatment of S2 cell nuclei, followed by polymerase chain reaction–free library construction on high–molecular-weight DNA extracted from either treated or untreated nuclei.

[1]Division of Genetics, Department of Medicine, Brigham and Women's Hospital, Harvard Medical School, Boston, MA, USA. [2]Department of Genetics, Blavatnik Institute, Harvard Medical School, Boston, MA, USA. [3]Altius Institute for Biomedical Sciences, Seattle, WA, USA. [4]Departments of Genome Sciences and Medicine, University of Washington, Seattle, WA, USA.
*Corresponding author. Email: absterga@u.washington.edu (A.B.S.); jstam@altius.org (J.A.S.)

Downloaded from https://www.science.org at Washington University on January 21, 2026

The resulting libraries were subjected to single-molecule CCS, providing very high base-calling accuracy (fig. S4, A and B) across chromatin fibers of up to ~30 kb in length (average fiber length, 10.9 kb) (Fig. 2B). Whereas untreated nuclei showed minimal m6A signal, nearly all fibers from m6A-MTase–treated cells demonstrated a high degree of m6A methylation (Fig. 2, C to E, and fig. S4A). The m6A-MTase–treated sample yielded an average coverage of 43 fibers for each DHS, with the average number of m6A-marked bases on each fiber overlapping a DHS mirroring the density of DNase I cleavages quantified by DNase I–seq from bulk nuclei (Fig. 2F). We observed marked clustering of adenine methylations into short contiguous regions spanning tens to hundreds of nucleotides, flanked by extended stretches of unmodified nucleotides (Fig. 2, D and E). Two categories of methylase-accessible DNA sequences (MADs) were evident: (i) sequence elements with an average length of 272 bp that coincided with DHSs and (ii) far more numerous shorter sequence elements with an average length of 67 bp and regularized spacing, paralleling the expected size and distribution of internucleosomal linker regions (*29*) (Fig. 2G and fig. S4D). m6A modifications were largely absent from nucleosome-wrapped DNA between linker regions (Fig. 2, D and E), consistent with the requirement of m6A-MTases for base flipping to modify adenines (*30*), which is likely suppressed by nucleosome wrapping. Notably, extended stretches of unmodified bases were absent from deproteinized chromatin fibers treated with m6A-MTases (fig. S5). Together, these results show that Fiber-seq accurately translates m6A single-molecule chromatin stencils into a linear, nucleotide-precise readout of the primary architecture of chromatin.

All-or-none actuation of regulatory DNA on individual fibers

We next sought to identify how regulatory information encoded in genomic DNA is actuated on individual chromatin fibers. Regulatory DNA actuation (the all-or-none adoption of a nucleosome-free state with resulting hyperaccessibility of the underlying DNA) is fundamental to cell state and fate decisions (*31*) as well as phenotypic traits and disease risk (*32*), yet it is currently unknown whether regulatory elements are actuated in an all-or-none fashion on any given chromatin fiber (in place of a canonical nucleosome) or whether regulatory DNA is actuated to varying degrees on all chromatin fibers as alternative structures with varying DNA accessibility. Evaluation of individual chromatin fibers overlapping each DHS demonstrated that overall, only 81% of these fibers had large MADs consistent with an actuated or open

Downloaded from https://www.science.org at Washington University on January 21, 2026

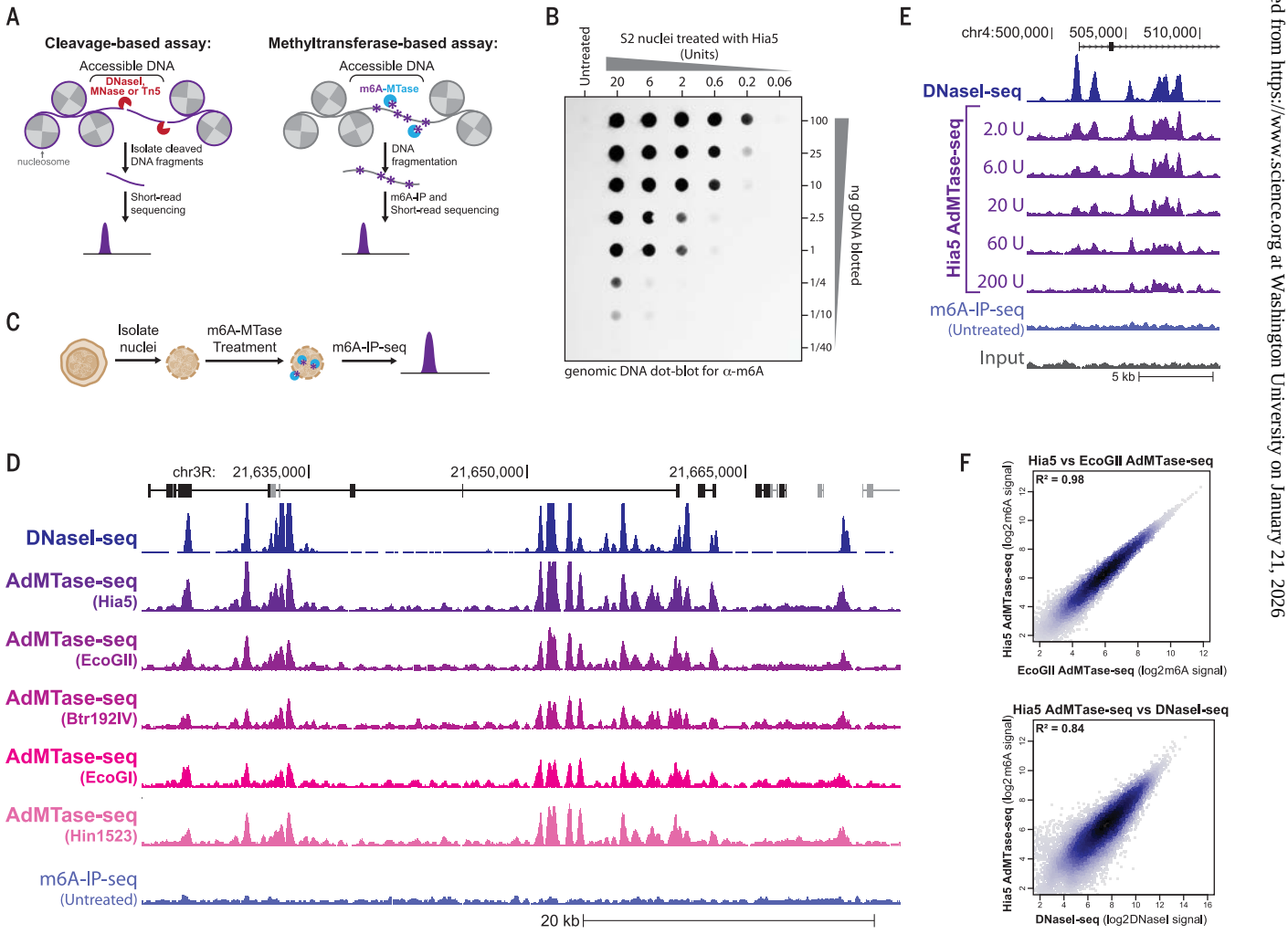

Fig. 1. Nonspecific m6A-MTases selectively mark sites of chromatin accessibility. (**A**) Schematic of cleavage- and m6A-MTase-based methods for marking sites of chromatin accessibility. Tn*5*, transposon 5. (**B**) Dot-blot quantification of m6A-modified genomic DNA (gDNA) from S2 cell nuclei after treatment with the m6A-MTase Hia5. (**C**) Experimental schematic for AdMTase-seq. (**D** and **E**) Genomic loci comparing the relationship between DNase I–seq signal and AdMTase-seq signal after treatment of S2 cell nuclei with (D) five separate m6A-MTases or (E) increasing amount of the m6A-MTase Hia5. The *y* axis is identical for all AdMTase-seq and m6A-immunoprecipitation-sequencing (m6A-IP-seq) experiments. (**F**) Comparison of AdMTase-seq signal for S2 cell DHSs from cells treated with (top) Hia5 versus EcoGII or (bottom) bulk DNase I–seq signal. The *y* axis is identical for all AdMTase-seq and m6A-IP-seq experiments.

chromatin state overlapping the DHS, with the remaining fibers showing nucleosome demarcation indicative of a closed state at the DHS (Fig. 3, A and B, and fig. S6, A to C). Transcription start site (TSS)–distal DHSs were preferentially maintained in a closed state when compared with promoter DHSs (Fig. 3B), and the rate of DNA actuation at individual TSS-distal DHSs mirrored the density of DNase I cleavages quantified by DNase I–seq from bulk nuclei (Fig. 3C). By contrast, wider TSS-distal DHSs, as well as promoter DHSs, were preferentially maintained in an accessible state (Fig. 3B and fig. S6D), with the actuated DNA content of these DHSs demonstrating widespread heterogeneity across individual chromatin fibers (Fig. 2, E and G) because of the variable punctuation of co-occupying nucleosomes (fig. S6E). Together, these findings demonstrate that the regulatory DNA content at TSS-distal regulatory elements is predominately modulated by all-or-none DNA actuation, with the regulatory DNA content at larger promoter elements additionally modulated by the variable punctuation of co-occupying nucleosomes.

Co-actuation of neighboring elements on single chromatin fibers

Linear clustering of gene regulatory elements along complex genomes is well described, canonically in the context of locus control regions (LCRs) or "super-enhancers" (e.g., the beta-globin LCR) or gene-specific control regions (e.g., the *BCL11A* enhancer region) (*33*–*36*). It is currently unknown whether the individual elements in such clusters are actuated coordinately or independently or, more generally, whether actuation of one genomic

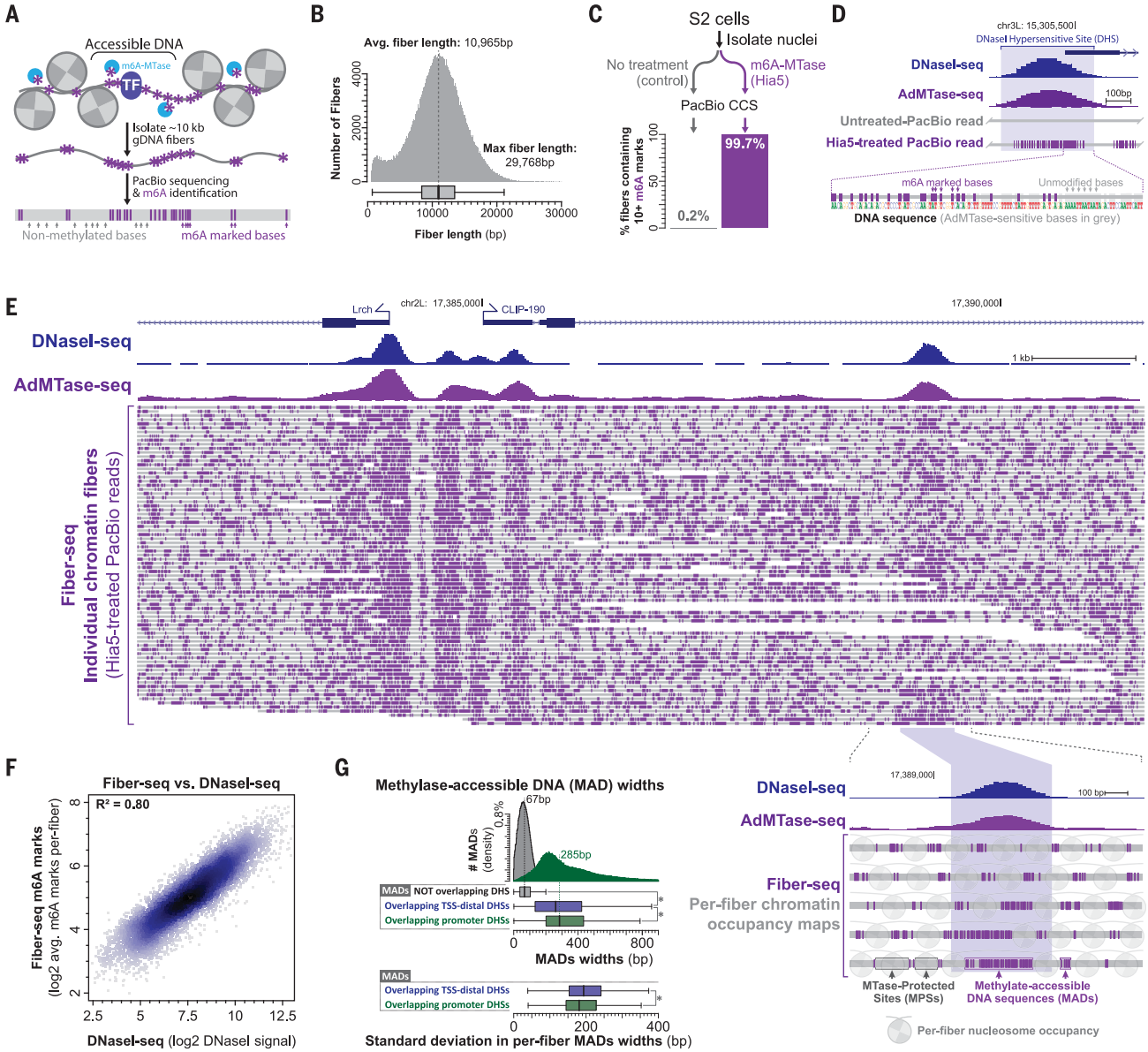

Fig. 2. Fiber-seq exposes base pair–resolution maps of individual chromatin fiber architecture. (**A**) Experimental schematic for Fiber-seq. (**B**) Histogram of read lengths for chromatin fibers sequenced using Fiber-seq. Avg., average. (**C**) Percentage of chromatin fibers with m6A-methylated bases from DNA isolated from untreated and Hia5-treated S2 cell nuclei. (**D** and **E**) Genomic loci comparing the relationship between DNase I–seq, AdMTase-seq, and Fiber-seq. Individual PacBio reads (chromatin fibers) are marked with gray lines, and m6A-modified bases are marked in purple dashes. White regions separate individual reads. Insets show (D) DHS with individual m6A-modified bases and (E) a comparison of multiple fibers overlapping a single DHS. (**F**) Scatterplot comparing DNase I–seq signal and the average Fiber-seq m6A signal at each DHS. (**G**) (Top) Histogram of MAD widths for all MADs identified outside of DHSs (gray) or in promoter DHSs (green). Box-and-whisker plots for the aforementioned in addition to MAD widths for all MADs identified in TSS-distal DHSs (blue). (Bottom) Box-and-whisker plots showing the standard deviation in MAD widths across multiple fibers overlapping a DHS. *P value < 0.001 (Wilcoxon test).

Downloaded from https://www.science.org at Washington University on January 21, 2026

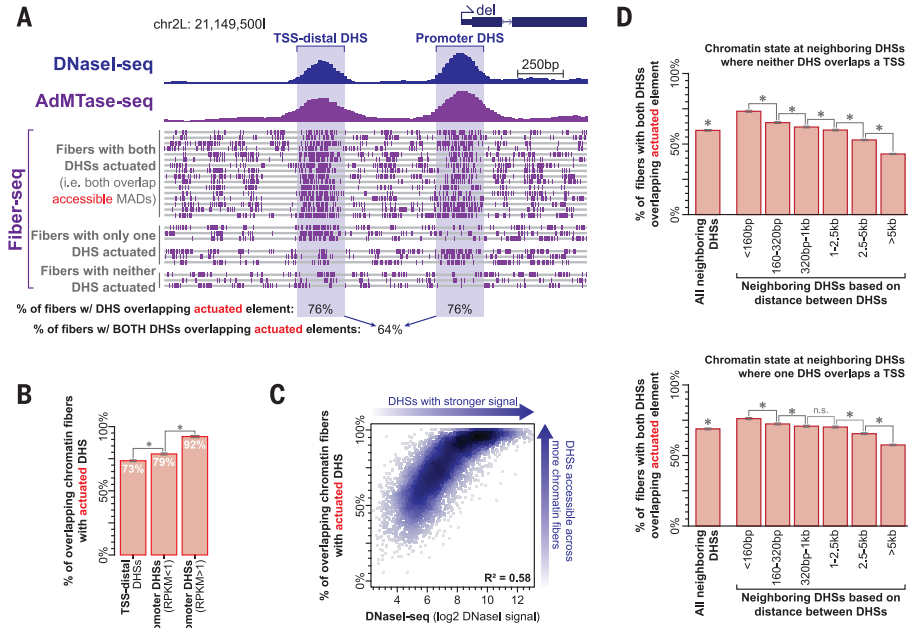

Fig. 3. Preferential co-actuation of neighboring regulatory elements on the same chromatin fiber. (**A**) Representative genomic locus comparing the relationship between DNase I–seq, AdMTase-seq, and Fiber-seq at neighboring DHSs exposes the predominant all-or-none actuation of individual DHSs. (**B**) Proportion of DHSs that overlap actuated versus closed fibers for DHSs divided based on their proximity to TSSs as well as the gene expression level of the TSS. Error bars represent 95% confidence intervals. *P value < 0.001 (z-test). RPKM, reads per kilobase per million reads. (**C**) Scatterplot showing the relationship between DHS actuation and the bulk DNase I–seq signal for TSS-distal DHSs. (**D**) For chromatin fibers encompassing two DHSs, shown is the percentage of fibers containing accessible MADs at both DHSs as a function of the distance between the DHSs. Error bars represent 95% confidence intervals. *P < 0.001 (z-test).

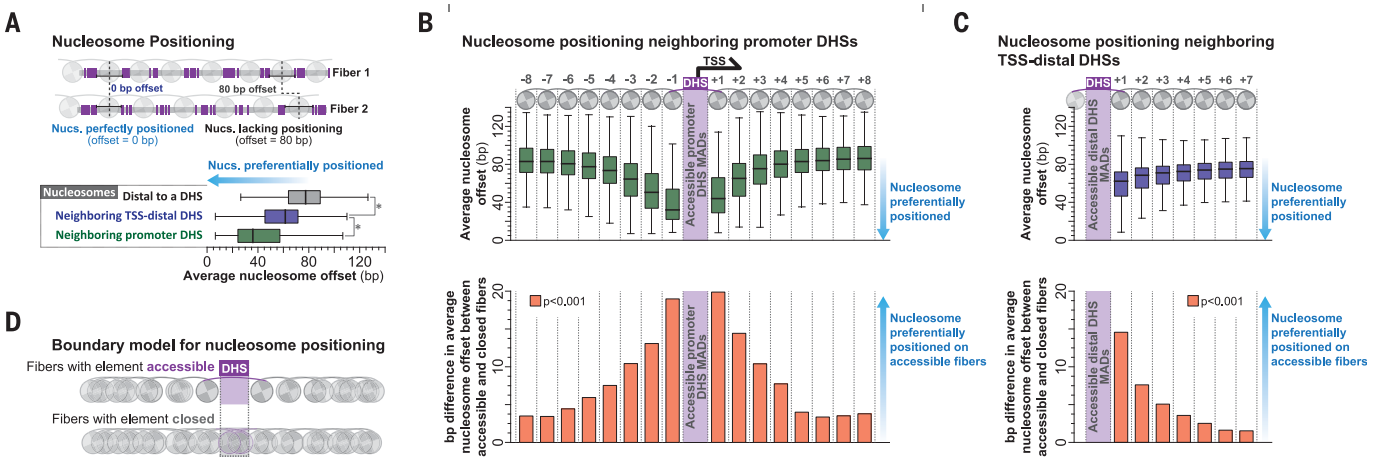

Fig. 4. Impact of regulatory DNA actuation on nucleosome positioning. (**A**) Schematic showing the calculation of nucleosome (Nucs.) positioning using overlapping reads as well as a box-and-whisker plot of nucleosome offsets at different genomic loci. *P value < 0.001 (Wilcoxon test). (**B** and **C**) (Top) Box-and-whisker plots showing nucleosome offsets neighboring (B) promoter DHSs and (C) TSS-distal DHSs. (Bottom) Bar plots demonstrating the difference in nucleosome positioning neighboring (B) promoter DHSs and (C) TSS-distal DHSs between actuated and closed fibers. P < 0.001 (Wilcoxon test). (**D**) Schematic of the boundary model for nucleosome placement surrounding regulatory elements.

element can influence actuation of neighboring elements. As 29% of Fiber-seq reads overlap multiple neighboring DHSs (Figs. 2E and 3A), we next asked whether regulatory DNA actuation at one genomic DNA element could influence the actuation of neighboring elements on the same chromatin fiber. Overall, we found that neighboring DHSs were significantly more likely to be co-actuated on the same chromatin fiber (Fig. 3D). Co-actuation was most strongly enriched for the most tightly clustered elements (Fig. 3D), indicating that the actuation of regulatory DNA accessibility at one distal element appears to potentiate accessibility at neighboring elements in a distance-dependent manner, independent of whether both elements were bound by the same TF (fig. S7). These results provide a possible physicochemical basis for the observed clustering of distal regulatory elements in animal genomes. Moreover, they suggest that genetic variants affecting regulatory DNA accessibility and function may create local knock-on effects in cis, a feature not accounted for in current models of the architecture and evolution of gene regulation.

Nucleosome arrays are bounded by actuated regulatory DNA

Nucleosome positioning is fundamental to gene regulation and is specified by a combination of factors, including DNA sequence, the competitive occupancy of TFs, the action of nucleosome remodelers, and interactions with RNA polymerases (*37*). Although nucleosomes surrounding accessible promoters and TSS-distal DHSs are generally well positioned (*38*–*40*), it remains unclear whether this positioning results from underlying nucleosome-favoring DNA sequences or from a boundary condition imposed by accessibility and TF occupancy at regulatory DNA. We reasoned that the boundary model of nucleosome positioning could be tested directly by comparing nucleosome positions surrounding a regulatory element on overlapping fibers in which the regulatory element is in an actuated or open state versus overlapping fibers in which the regulatory element is in a closed state (as such fibers have the same DNA content and should differ only in the presence or absence of an actuated element). Although nucleosomes

Downloaded from https://www.science.org at Washington University on January 21, 2026

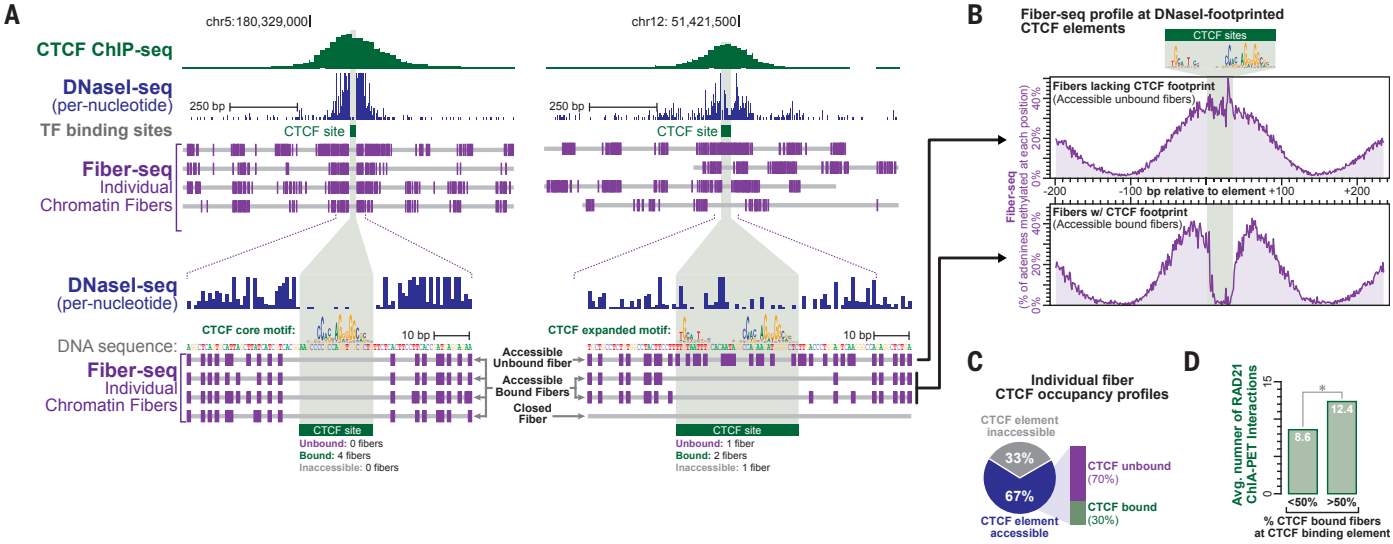

Fig. 5. Heterogeneous single-molecule CTCF occupancy impacts long-range CTCF interactions. (**A**) Genomic loci comparing the relationship between CTCF chromatin immunoprecipitation sequencing (ChIP-seq), DNase I–seq, and Fiber-seq at CTCF binding sites in K562 cells. The inset shows a CTCF binding site and per-fiber m6A methylation. (**B**) Plot of adenine methylation frequency surrounding DNase I–footprinted CTCF binding sites for individual fibers that (top) lack a CTCF footprint or (bottom) have a CTCF footprint. (**C**) Percentage of fibers overlapping CTCF ChIP-seq peaks containing a bulk CTCF DNase I footprint that lack an accessible MADs or have an accessible MADs with or without a CTCF footprint. (**D**) Average number of RAD21 ChIA-PET long-range chromatin interactions at CTCF binding sites based on the percentage of overlapping fibers that contain a single-molecule CTCF footprint. *P value < 0.01 (z-test).

surrounding DHSs were collectively well positioned (Fig. 4A), analysis of single-fiber data showed that well-positioned nucleosomes largely originated from fibers in which the regulatory element is in an actuated state (Fig. 4, B and C), indicating that nucleosome positioning at these locations is largely dependent on the actuation of regulatory DNA, not the DNA sequence itself. As such, nucleosome positioning appears to largely result from a boundary condition imposed by regulatory DNA actuation on individual chromatin fibers (Fig. 4D).

Fiber-seq of human chromatin

To test Fiber-seq on the human genome, we first validated that m6A-MTases can selectively mark cell type–specific accessible DNA in human cell types (fig. S8A). We then performed Fiber-seq on human K562 nuclei, resulting in robust demarcation of both accessible regulatory elements and internucleosomal linker regions (fig. S8, B to E) with an average coverage of 3.7 high-quality reads per DHS. Consistent with the findings from *Drosophila* cells, we found that regulatory DNA accessibility in K562 cells is predominantly actuated as an all-or-none process (fig. S8F), with larger promoter elements additionally demonstrating variably placed co-occupying nucleosomes (fig. S8G). Furthermore, neighboring TSS-distal DHSs were significantly more likely to be co-actuated on the same chromatin fiber (fig. S8H), and nucleosome positioning surrounding regulatory DNA was largely dependent on regulatory DNA accessibility as a boundary condition (fig. S8, I and J), indicating that these are likely universal effects of regulatory DNA actuation.

Single-molecule TF occupancy at nucleotide resolution

Analysis of K562 Fiber-seq patterns in accessible regulatory elements revealed that m6A-MTase methylation was not uniform but rather was punctuated by short gaps, consistent with nucleotide-precise binding of TFs that mirror bulk TF footprints on non–cross-linked chromatin (Fig. 5, A and B, and fig. S9) (*41*). We next explored these single-molecule TF occupancy events to determine the relationship between TF occupancy and regulatory DNA actuation and function, focusing on CTCF because most of its binding sites lack additional co-bound TFs, and CTCF occupancy is considered essential for establishing long-range chromatin interactions (*42*). TFs are known to undergo rapid exchange at regulatory DNA elements (*43*), yet it remains unclear the extent to which regulatory elements can remain actuated during the transient absence of TF occupancy (*44*–*46*). We observed that most of the actuated chromatin fibers overlapping CTCF-bound regulatory elements lacked a CTCF footprint (Fig. 5, B and C), suggesting that regulatory DNA actuation can be maintained in the absence of immediate occupancy by a gating TF. Notably, CTCF elements that preferentially contained fibers with a CTCF footprint were more likely to participate in long-range chromatin interactions (Fig. 5D), providing a mechanistic link between single-molecule CTCF occupancy and function.

Outlook

In conclusion, we have shown that Fiber-seq provides a robust and scalable approach for stenciling the primary architecture of individual chromatin fibers onto their underlying DNA templates with high precision and resolution. As both sequencing read lengths and throughput increase, it should be possible in the near future to transcribe and resolve the primary regulatory architectures of entire genetic haplotypes by simultaneously mapping both the primary genetic sequence and overlying chromatin state. As such, Fiber-seq has the potential to provide a unifying tool for analyzing the gene regulatory impact of both rare and common regulatory DNA variation, and for resolving extended regulatory alleles.

REFERENCES AND NOTES

1. D. S. Gross, W. T. Garrard, *Annu. Rev. Biochem.* **57**, 159–197 (1988).
2. R. E. Thurman *et al.*, *Nature* **489**, 75–82 (2012).
3. M. Noll, R. D. Kornberg, *J. Mol. Biol.* **109**, 393–404 (1977).
4. D. E. Schones *et al.*, *Cell* **132**, 887–898 (2008).
5. E. Lieberman-Aiden *et al.*, *Science* **326**, 289–293 (2009).
6. J. D. Buenrostro, P. G. Giresi, L. C. Zaba, H. Y. Chang, W. J. Greenleaf, *Nat. Methods* **10**, 1213–1218 (2013).
7. T. Kouzarides, *Cell* **128**, 693–705 (2007).
8. T. K. Kelly *et al.*, *Genome Res.* **22**, 2497–2506 (2012).
9. A. R. Krebs *et al.*, *Mol. Cell* **67**, 411–422.e4 (2017).
10. N. H. Nabilsi *et al.*, *Genome Res.* **24**, 329–339 (2014).
11. Y. Wang *et al.*, *Genome Res.* **29**, 1329–1342 (2019).
12. Z. Shipony *et al.*, *Nat. Methods* **17**, 319–327 (2020).
13. A. P. Bird, *Nature* **321**, 209–213 (1986).
14. K. Tanaka, A. Okamoto, *Bioorg. Med. Chem. Lett.* **17**, 1912–1915 (2007).
15. A. B. R. McIntyre *et al.*, *Nat. Commun.* **10**, 579 (2019).
16. G. Z. Luo, C. He, *Nat. Struct. Mol. Biol.* **24**, 503–506 (2017).
17. J. Singh, A. J. S. Klar, *Genes Dev.* **6**, 186–196 (1992).
18. D. E. Gottschling, *Proc. Natl. Acad. Sci. U.S.A.* **89**, 4062–4065 (1992).
19. M. P. Kladde, R. T. Simpson, *Proc. Natl. Acad. Sci. U.S.A.* **91**, 1361–1365 (1994).

Downloaded from https://www.science.org at Washington University on January 21, 2026

20. M. Drozdz, A. Piekarowicz, J. M. Bujnicki, M. Radlinska, *Nucleic Acids Res.* **40**, 2119–2130 (2012).
21. B. P. Anton, G. P. Harhay, T. P. L. Smith, J. Blom, R. J. Roberts, *PLOS ONE* **11**, e0161499 (2016).
22. I. A. Murray *et al*., *Nucleic Acids Res.* **46**, 840–848 (2018).
23. G. Fang *et al*., *Nat. Biotechnol.* **30**, 1232–1239 (2012).
24. H. Weintraub, M. Groudine, *Science* **193**, 848–856 (1976).
25. K. S. Bloom, J. N. Anderson, *Cell* **15**, 141–150 (1978).
26. J. Mieczkowski *et al*., *Nat. Commun.* **7**, 11485 (2016).
27. J. Eid *et al*., *Science* **323**, 133–138 (2009).
28. K. J. Travers, C. S. Chin, D. R. Rank, J. S. Eid, S. W. Turner, *Nucleic Acids Res.* **38**, e159 (2010).
29. R. V. Chereji *et al*., *Nucleic Acids Res.* **44**, 1036–1051 (2016).
30. J. R. Horton, K. Liebert, M. Bekes, A. Jeltsch, X. Cheng, *J. Mol. Biol.* **358**, 559–570 (2006).
31. A. B. Stergachis *et al*., *Cell* **154**, 888–903 (2013).
32. M. T. Maurano *et al*., *Science* **337**, 1190–1195 (2012).
33. W. A. Whyte *et al*., *Cell* **153**, 307–319 (2013).
34. P. Diaz, D. Cado, A. Winoto, *Immunity* **1**, 207–217 (1994).
35. L. Madisen, M. Groudine, *Genes Dev.* **8**, 2212–2226 (1994).
36. F. Grosveld, G. B. van Assendelft, D. R. Greaves, G. Kollias, *Cell* **51**, 975–985 (1987).
37. K. Struhl, E. Segal, *Nat. Struct. Mol. Biol.* **20**, 267–273 (2013).
38. S. Baldi *et al*., *Mol. Cell* **72**, 661–672.e4 (2018).
39. G.-C. Yuan *et al*., *Science* **309**, 626–630 (2005).
40. C. Jiang, B. F. Pugh, *Nat. Rev. Genet.* **10**, 161–172 (2009).
41. S. Neph *et al*., *Nature* **489**, 83–90 (2012).
42. J. E. Phillips, V. G. Corces, *Cell* **137**, 1194–1211 (2009).
43. T. C. Voss *et al*., *Cell* **146**, 544–554 (2011).
44. C. C. Adams, J. L. Workman, *Mol. Cell. Biol.* **15**, 1405–1421 (1995).
45. J. A. Miller, J. Widom, *Mol. Cell. Biol.* **23**, 1623–1632 (2003).
46. L. A. Mirny, *Proc. Natl. Acad. Sci. U.S.A.* **107**, 22534–22539 (2010).
47. A. B. Stergachis, Code for mapping single-molecule m6A methylations, Zenodo (2020); doi: 10.5281/zenodo.3743228

ACKNOWLEDGMENTS

We thank M. Radlinska for kindly providing the Hia5 and Hin1523 plasmids (*20*). We also thank L. Tallon and L. Sadzewicz for their assistance in PacBio sequencing as well as R. S. Isaac for his help with FPLC purification of the Hia5 enzyme. **Funding:** This work was supported by NIH grants UM1HG009444 to J.A.S. and T32GM007748 supporting A.B.S. **Author contributions:** A.B.S., B.M.D., and J.A.S. designed the experiments. A.B.S. and B.M.D. performed the experiments. A.B.S. and E.H. performed the computational analyses. A.B.S., B.M.D., and J.A.S. wrote the manuscript. L.S.C. provided ongoing support and many helpful critiques. **Competing interests:** A.B.S. and J.A.S. are coinventors on U.S. patent application 63/004,361 that includes discoveries described in this manuscript. **Data and materials availability:** All data are available in the manuscript or the supplementary materials or at GEO accession GSE146942. Code for generating single-fiber chromatin architectures is available at Zenodo.org (*47*).

SUPPLEMENTARY MATERIALS

science.sciencemag.org/content/368/6498/1449/suppl/DC1
Materials and Methods
Figs. S1 to S9
References (*48*–*54*)
MDAR Reproducibility Checklist

View/request a protocol for this paper from *Bio-protocol*.

17 August 2019; resubmitted 12 January 2020
Accepted 24 April 2020
10.1126/science.aaz1646

Downloaded from https://www.science.org at Washington University on January 21, 2026